ACSNANO

www.acsnano.org

ARTICLE

Gold Nanoparticles Inhibit Macropinocytosis by Decreasing KRAS Activation

Chandra Kumar Elechalawar, Geeta Rao, Suresh Kumar Gulla, Maulin Mukeshchandra Patel, Alex Frickenstein, Nicolas Means, Ram Vinod Roy, Leonidas Tsiokas, Sima Asfa, Prasanta Panja, Chinthalapally Rao, Stefan Wilhelm, Resham Bhattacharya, and Priyabrata Mukherjee*

Cite This: https://doi.org/10.1021/acsnano.3c00920

Read Online

ACCESS | Metrics & More | Article Recommendations | Supporting Information

ABSTRACT: **The RAS-transformed cells utilize macropinocytosis to acquire amino acids to support their uncontrolled growth. However, targeting RAS to inhibit macropinocytosis remains a challenge. Here, we report that gold nanoparticles (GNP) inhibit macropinocytosis by decreasing KRAS activation. Using surface-modified and unmodified GNP, we showed that unmodified GNP specifically sequestered both wild-type and mutant KRAS and inhibited its activation, irrespective of growth factor stimulation, while surface-passivated GNP had no effect. Alteration of KRAS activation is reflected on downstream signaling cascades, macropinocytosis and tumor cell growth *in vitro*, and two independent preclinical human xenograft models of pancreatic cancer *in vivo*. The current study demonstrates NP-mediated inhibition of macropinocytosis and KRAS activation and provides translational opportunities to inhibit tumor growth in a number of cancers where activation of KRAS plays a major role.**

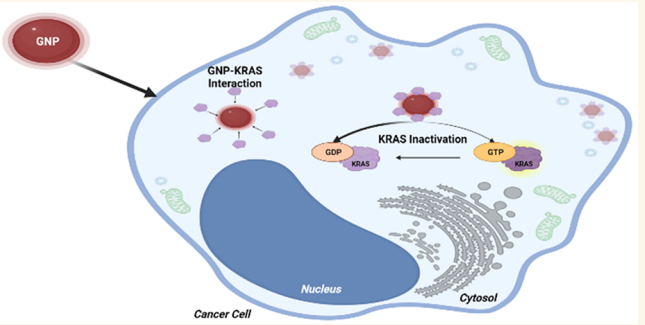

KEYWORDS: *gold nanoparticles, macropinocytosis, KRAS, pancreatic ductal adenocarcinoma, RAS*

INTRODUCTION

Macropinocytosis is a conserved nonselective endocytosis process exploited by diverse cell types to ingest extracellular fluid, macromolecules, and/or cell/tissue necrotic debris for cellular homeostasis.[1−3] Intracellular pathogens such as viruses, for example, utilize macropinocytosis to enter into the cytoplasm to hijack the host cell machineries to propagate. Immune cells such as dendritic cells and macrophages, however, exploit macropinocytosis for optimum antigen presentation and cell migration.[4,5] Cancer cells, RAS-transformed cells in particular, on the other hand aberrantly activate macropinocytosis, utilizing it as a nutrient uptake pathway to acquire amino acids to support their incessant proliferative potential.[1,6] Once taken up by the cells, extracellular proteins and other macromolecules are transported to lysosomes and degraded to produce amino acids and other constituents supporting cellular growth.[1,3] RAS-transformed pancreatic ductal adenocarcinoma (PDAC) cells exploit macropinocytosis to internalize extracellular albumin to generate amino acids to contribute to the intracellular amino acid pools and to the biosynthesis of central carbon metabolites. Macropinocytosis is found to be prevalent in PDAC human and mouse tumors of both xenograft and autochthonous origin. Cells within the tumor microenvironment, such as tumor-associated fibroblasts, also utilize macropinocytosis to support tumor growth.[7,8] However, effective strategies to inhibit macropinocytosis and tumor growth by targeting activation of KRAS are challenging.[9,10] Approaches based on nanoparticle (NP) technology have the potential to address this challenge.

Among all NP used in various biological application, gold NP (GNP) have a particular binding affinity for thiol (−SH)- and amine ($-NH_2$)-containing molecules through Au−SH and Au−NH_2 interactions.[11] All NP, including GNP, when exposed to biological fluids form a biological coat, termed the biomolecular corona.[12] The biomolecular corona around GNP has been exploited to identify new molecular targets in cancer and other diseases.[13] Previously, we reported that GNP bind to heparin-binding growth factors (HB-GFs) through the HB-domain and inhibit their function by alteration of protein

Received: January 31, 2023
Accepted: April 27, 2023

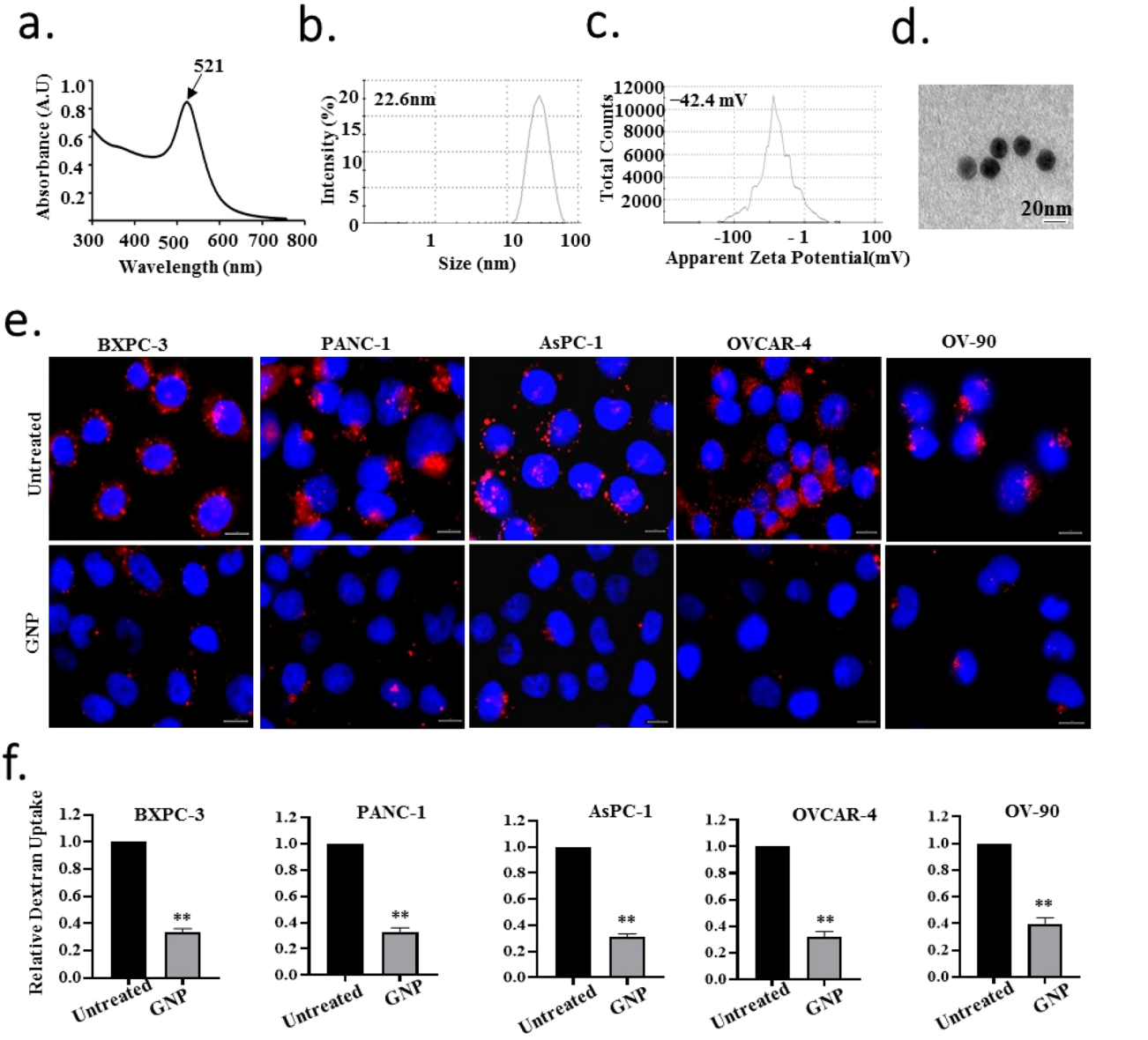

Figure 1. GNP inhibit macropinocytosis in cancer cells. (a−d) Physicochemical characterization of GNP using (a) UV−visible absorbance spectrum and their absorbance maxima (λ_{max}). (b) DLS (nm). (c) Zeta potential (ζ). (d) Transmission electron micrograph (TEM) analysis, scale bar = 20 nm. (e) GNP treatment inhibits TMR-dextran uptake (a marker of macropinocytosis) in BXPC-3, PANC-1 AsPC-1, OVCAR-4, and OV-90 cancer cells. After 48 h of GNP treatments, TMR-dextran (red) was added to the cells. Cell nuclei were stained using DAPI (blue staining). Scale bar represents 10 μm. (f) Quantification of macropinosomes using ImageJ software. Mean ± SD, $^{**}P < 0.1$. Results obtained are representative of three experiments.

conformation, whereas GNP had no effect on non-HB-GFs.[14,15] In addition, ourselves and others also reported that GNP inhibit tumor growth, metastasis, and therapy resistance in a number of malignancies including pancreatic and ovarian cancer.[14] Furthermore, among different sizes of GNP tested, 20 nm GNP exhibited the highest biological efficacy. However, whether such properties of GNP could be utilized to inhibit KRAS activation and macropinocytosis has not yet been studied. Using a series of *in vitro* and *in vivo* experiments we investigated, in the current study, whether GNP treatment could regulate KRAS activation and macropinocytosis, and whether surface passivation of GNP by PEGylated-thiols could interfere with such effects.

RESULTS/DISCUSSION

Synthesis and Characterization of GNP. In the present study we used GNP of 20 nm size, since previous reports demonstrated that GNP of 20 nm size have the highest efficacy to inhibit tumor cell growth.[14,16] We synthesized GNP by the citrate reduction method as reported previously[14] and characterized them by UV−visible spectroscopy (UV−vis), dynamic light scattering (DLS), zeta potential measurements, and transmission electron microscopy (TEM) (Figure 1a−1d). UV−vis spectra exhibited a surface plasmon resonance (SPR) peak at ∼521 nm, indicating formation of spherical GNP by this method (Figure 1a). Hydrodynamic diameter (HD) and charge of as-synthesized GNP were determined to be 24 nm (Figure 1b) and −43 mV (Figure 1c), respectively, as evidenced by DLS and zeta potential measurements. The

https://doi.org/10.1021/acsnano.3c00920
ACS Nano XXXX, XXX, XXX−XXX

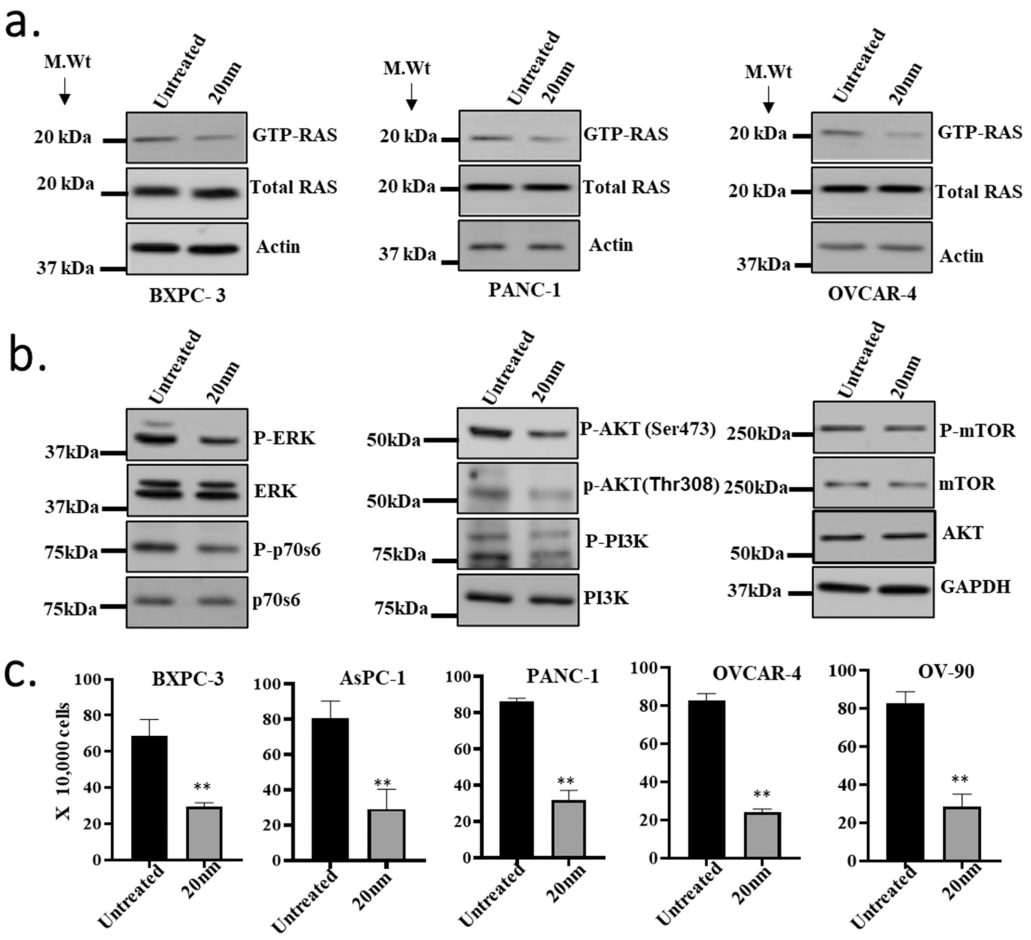

Figure 2. GNP treatment downregulates GTP-RAS activation, which turns down KRAS downstream signaling. (a) GNP treatments decreased activated RAS (GTP-RAS) levels but not total RAS in BXPC-3, PANC-1, or OVCAR-4 cells. After 48 h of treatments, lysates were collected for activated GTP-RAS pull-down assay. (b) Downregulation of RAS downstream signaling in PANC-1 cell lysates was determined using Western blot analysis through immunoblotting of Phosho-ERK, ERK, Phospho-p70S6, p-70S6, Phospho-AKT (Ser473), Phospho-AKT (Thr308), AKT, Phospho-PI3K, PI3K, Phospho-mTOR, and mTOR. (c) Inhibition of RAS downstream signaling with GNP led to reduced proliferation of cancer cells. Mean ± SD, $^{**}P < 0.1$. All data are representative of two or three independent experiments.

core size of GNP was further confirmed by TEM, showing GNP of ~20 nm were formed by this method (Figure 1d). After thorough physicochemical characterization of synthesized GNP, we then sought to investigate their ability to regulate macropinocytosis.

Impact of GNP Treatment on Macropinocytosis of Cancer and Normal (Mouse Embryonic Fibroblast) Cells. Macropinocytosis is usually studied by uptake of fluorescently labeled dextran (TMR-dextran, MW 70 KD) or albumin (BSA-Alexa Fluor-488).[17] To demonstrate biological relevance and generality, we selected a number of PDAC cells harboring both wild-type (BXPC-3) and mutant KRAS (PANC-1 and AsPC-1) as well as the ovarian cancer cells OVCAR-4 and OV-90. GNP treatment drastically inhibited uptake of TMR-dextran, as visualized by the fluorescence images captured by Zeiss Epifluoresence microscopy (Figure 1e). Quantification of the TMR-dextran uptake revealed nearly 60−80% inhibition of TMR-dextran uptake by GNP treatment in all the cell types compared to nontreated controls (Figure 1f). Furthermore, we have performed dextran uptake in PANC-1 cells with the macropinocytosis inhibitor[7] *N*-(ethyl-*N*-isopropyl)amiloride (EIPA) as positive control. We observed a significant reduction in dextran uptake in both the GNP-treated and the EIP-treated groups (Figure S9), supporting a role of GNP as an inhibitor of macropinocytosis.

Since cargoes are transported to lysosomes after macropinocytotic uptake for degradation,[18] next we investigated uptake of BSA-Alexa Fluor-488 and its colocalization with the lysosome after labeling of the lysosome with Lysotracker-DND99. GNP treatment profoundly inhibited BSA uptake and its colocalization with the lysosome as visualized by fluorescence microscopy (Figure S1), further confirming inhibition of macropinocytosis by GNP. Furthermore, to demonstrate specificity of GNP toward macropinocytosis inhibition, we investigated intracellular uptake of transferrin in PANC-1 cells using Alexa-Fluor 488-tagged transferrin. Cellular internalization of transferrin occurs through clathrin-mediated endocytosis (CME).[19] Fluorescence microscopy images revealed that GNP treatment did not inhibit CME uptake of transferrin (Figure S2), while an inhibitor of the CME pathway, chloropromazine (CMZ), completely inhibited it (Figure S2). Taken together, results from the dextran, BSA, and transferrin uptake studies support that GNP specifically inhibit macropinocytosis but not CME. To further evaluate the impact of GNP on macropinocytosis in normal cells, we treated NIH3T3 cells (mouse embryonic fibroblasts) with GNP and measured dextran uptake as we did in the case of

https://doi.org/10.1021/acsnano.3c00920
ACS Nano XXXX, XXX, XXX−XXX

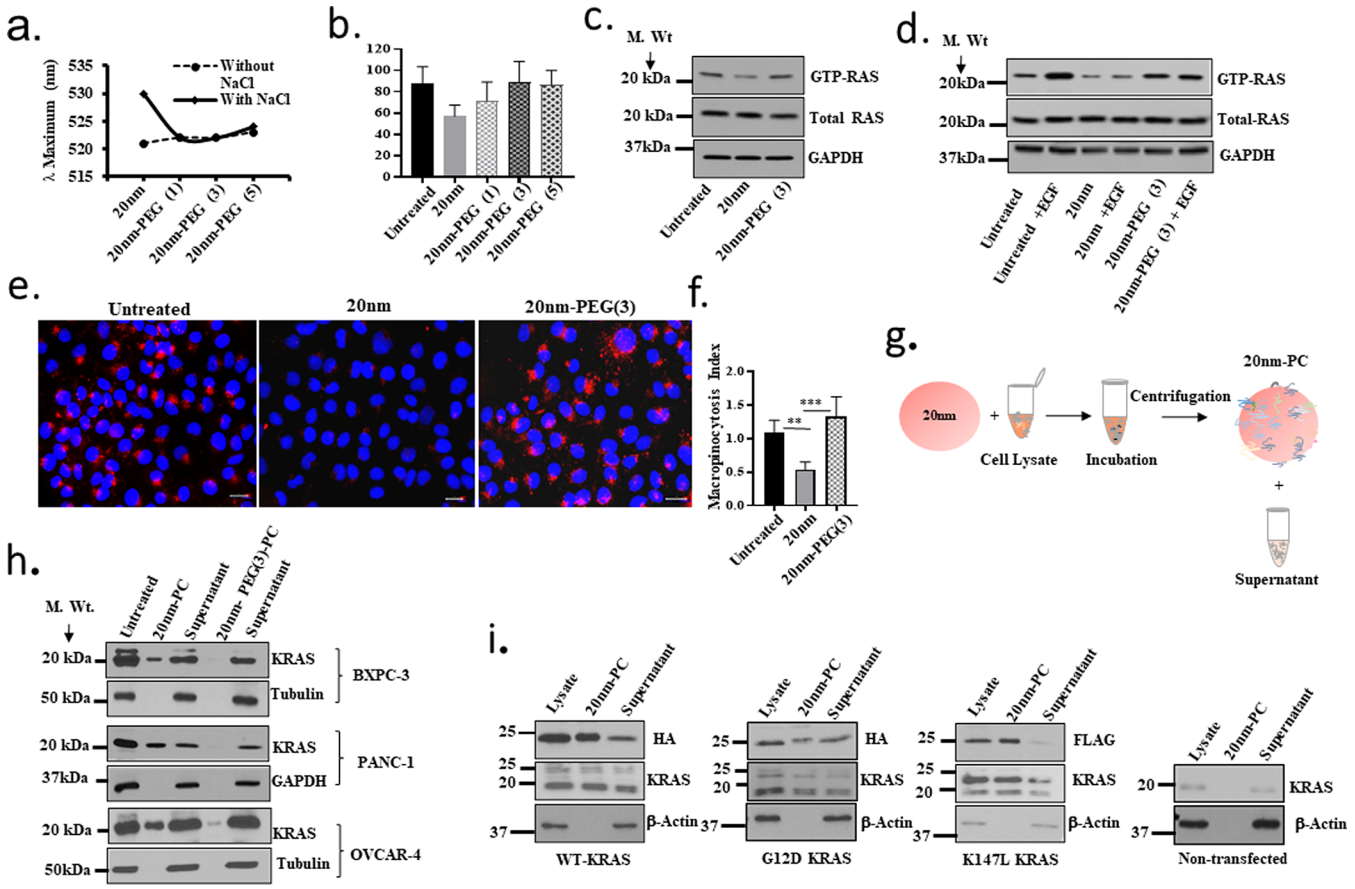

Figure 3. A bare surface is important for GNP to show their biological activity. (a) GNP were subjected to complete surface coverage using the PEGylation strategy by addition of various concentrations of methoxy-PEG (1000)-SH. Their surface coverage was confirmed by formation of nonaggregated GNP following addition of 150 mM NaCl solution. (b) PEGylated GNP did not inhibit the proliferation of PANC-1 cells, while proliferation inhibition is present with non-PEGylated GNP treatments. (c) Downregulation of RAS activation using GNP was rescued with post surface coverage of GNP using a GTP-RAS pulldown assay. (d) In GNP-pretreated PANC-1 cells, pulsing with epidermal growth factor (EGF) did not activate the GTP-RAS, whereas in untreated cells EGF pulsing did significantly increase the GTP-RAS level, showing a potential effect on GTP-RAS activation downregulation by GNP in the presence of growth factors. (e) Passivated GNP or PEGylated GNP did not show TMR-dextran uptake inhibition, illustrating the importance of a GNP bare surface to their macropinocytosis inhibition effect or biological activity in cancer cells; scale bar = 20 μm. (f) Quantification of TMR-dextran uptake using ImageJ software analysis, $^{**}P < 0.1$, $^{***}P < 0.001$. *P* values were calculated using one-way ANOVA. (g) GNP were able to pull down KRAS protein from the BXPC-3, PANC-1, and OVCAR-4 cell lysates, whereas PEGylated GNP did not pull down KRAS. 50 μg of either GNP or PEGylated GNP was incubated with 200 μg of corresponding cell lysates on an end-over-end rotator for 18 h followed by centrifugation to separate the biomolecular corona around GNP (GNP-PCs). 15 μg of proteins from lysates, GNP-PC, PEGylated GNP, and their corresponding supernatants was separately loaded in 12% gel for Western blot analysis using anti-KRAS antibody. (h) GNP do not show specificity toward pulling down particular KRAS mutants: WT-KRAS, G12D-KRAS, and K147L-KRAS. Following transfection of WT-KRAS, G12D-KRAS, and K147L-KRAS plasmids in HEK-293 cells, lysates were collected. The biomolecular protein corona around GNP was prepared and isolated as described earlier by incubating the cell lysates with GNP followed by separation and Western blot analysis to test the specificity of GNP toward specific KRAS mutants.

cancer cells (Figure S10). The results demonstrated that GNP treatment inhibited the macropinocytotic uptake of dextran in NIH-3T3 cells, albeit with lower efficiency. These results suggest that macropinocytosis plays a more prominent role in epithelial cancer cells as compared with normal cells. Next, we sought to investigate mechanisms through which GNP inhibit macropinocytosis.

Impact of GNP Treatment on KRAS Activation in Cancer Cells. It is reported that RAS-transformed PDAC cells rely on macropinocytosis to meet the metabolic requirement for uncontrolled growth.[1,20] Therefore, we sought to investigate if GNP treatment inhibited KRAS activation in these cells in order to inhibit macropinocytosis. We used BXPC-3, PANC-1, and OVCAR-4 cells as a proof-of-concept study. GTP-bound RAS (activated RAS) was pulled down in GNP-treated and nontreated cells, and expression of GTP-RAS was determined by immunoblot analyses. In all the cell types tested, GNP treatment inhibited expression of activated RAS (GTP-RAS) proteins, while the expression of total RAS protein did not change (Figure 2a). These results suggest that the inhibition of macropinocytosis by GNP treatment is due to the inhibition of RAS activation. Next, we also tested the effect of GNP on the RAS regulators RAS-GAP and RAS-GEF (SOS1) as a possible mechanism of GNP-mediated regulation of RAS activation. We selected PANC-1 and BXPC-3 cells harboring mutant KRAS and wild-type KRAS, respectively, treated the cells with GNP, and probed for RAS-GAP and RAS-GEF expressions. GNP treatment did not, however, alter the expression levels of these regulators in PANC-1 and BXPC-3 cells (Figure S3), ruling out the possible involvement

https://doi.org/10.1021/acsnano.3c00920
ACS Nano XXXX, XXX, XXX−XXX

of RAS-GAP and RAS-GEF in GNP-mediated regulation of RAS activation.

RAS activation is known to stimulate a large number of downstream signaling cascades such as MAPK, AKT, and mTOR.[9,21] Therefore, we next investigated whether inhibition of RAS activation was reflected in the activation of its downstream effectors. We treated PANC-1 cells with GNP and probed for RAS downstream effectors by immunoblot analysis. Immunoblot analysis revealed that GNP treatment decreased activation of MAPK, AKT, mTOR, and p-70S6 kinase, all downstream effectors of the RAS signaling cascade (Figure 2b).[21,22] These results collectively further support that the GNP-mediated inhibition of macropinocytosis occurs due to the inhibition of RAS activation via signaling through the downstream effector molecules. Since activations of MAPK, AKT, and mTOR are major signaling nodes through which cancer cells proliferate and survive, next we investigated the impact of GNP treatment on cancer cell phenotypes, mainly proliferation.

Cell proliferation was measured by cell counting by the trypan blue method as described previously.[23] Nearly 60−80% inhibition of proliferation in all the cancer cell lines tested was seen following GNP treatment when compared with non-treated controls (Figure 2c). All of the results taken together suggest that GNP treatment inhibits macropinocytosis and cancer cell proliferation by decreasing RAS activation and RAS signaling cascades. Since we used as-synthesized GNP prepared by the citrate reduction method, we next wanted to investigate if the GNP surface played any crucial role in inhibiting macropinocytosis.

Impact of Surface Modifications of GNP on RAS Activation, Macropinocytosis, and Cellular Phenotypes. In order to address the involvement of the GNP surface in regulation of RAS activation, we passivated the GNP surface using methoxy-polyethylene glycol-SH having a molecular weight of 1000 Da (PEGs). First, we determined the saturation concentration of PEG to completely passivate the GNP surface by monitoring the SPR band in an aggregation assay with sodium chloride (NaCl).[24] Addition of increasing amounts of PEG (1, 3, and 5 μg per mL of GNP) caused a red shift in the SPR band and dampening of the absorption, indicating adsorption of PEG on the GNP surface (Figure 3a and Figure S4). Addition of 150 mM NaCl shifted the SPR band of as-synthesized GNP from ∼520 nm to ∼530 nm, indicating aggregation of GNP. However, addition of PEG protected the GNP surface from NaCl-induced aggregation, as evidenced by a marginal shift in SPR maxima where it plateaued at ∼520 nm (Figure 3a) following addition of 1−3 μg of PEG per mL of GNP. Thus, these aggregation studies reveal that 1−3 μg of PEG per mL of GNP is the saturation concentration. Binding of PEG to the GNP surface was further supported by an increase in hydrodynamic diameter from ∼22 nm to ∼40 nm and a decrease in charge from ∼−40 mV to ∼−14 mV (Figure S4). PEG binding to GNP was further confirmed by TEM, showing a contrast layer of PEG surrounding the GNP. Next, we investigated the impact of surface-passivated GNP on cellular proliferation using the cell counting method as described earlier. Among 1, 3, and 5 μg of PEG used to passivate 1 mL of GNP solution, 3 and 5 μg of PEG-passivated GNP had little effect in inhibiting cancer cell proliferation when compared with non-PEGylated GNP (Figure 3b). These results suggest that 3 μg of PEG is enough to saturate the surface of 1 mL of 20 nm GNP and block its inhibitory function. Since GNP-mediated decreases in RAS activation have been implicated above in inhibiting macropinocytosis and cellular proliferation, next we investigated the impact of surface PEGylation of GNP on the ability to decrease RAS activation. As a proof-of-principle study, GTP-bound RAS (activated RAS) was pulled down in PANC-1 cells as above, following treatment with both PEGylated and non-PEGylated as-synthesized GNP. This GTP-RAS pull-down assay demonstrated that PEGylated GNP could not inhibit RAS activation as compared to as-synthesized non-PEGylated GNP, which significantly decreased it (Figure 3c). Neither PEGylated nor non-PEGylated GNP had any impact on the expression of the total RAS proteins (Figure 3c). Taken together these results support that the GNP surface plays a critical role in inhibiting RAS activation. Since growth factors (GFs) are known to activate RAS and its downstream signaling, next we investigated the impact of GNP treatment on GF-induced activation of RAS.

Previously, we reported that GNP bind HB-GFs and inhibit their function by alteration of protein conformation, whereas conformation and function of non-HB-GFs remain unaffected.[14] Therefore, we chose to stimulate PANC-1 cells with EGF (non-HB-GF) and probe RAS activation with and without GNP treatment. It was expected that EGF stimulation would enhance RAS activation and that GNP would not have the ability to inhibit it. However, inhibition of RAS activation by GNP, even after EGF stimulation, would demonstrate a GF-independent inhibition of RAS activation and suggest that interaction of GNP with RAS may be playing an important role. EGF stimulation enhanced expression of GTP-RAS, as expected. Interestingly, GNP treatment inhibited RAS-GTP expression at the basal level as well as after EGF stimulation (Figure 3d). Importantly, surface PEGylation of GNP could not inhibit GTP-Ras expression either at the basal level or after EGF stimulation (Figure 3d). These results indicate that GNP-mediated inhibition of RAS activation is GF-independent and that the unmodified GNP surface plays a critical role.

After determining the role of surface PEGylation of GNP on RAS activation, we next investigated its impact on macropinocytosis. As observed with RAS activation, while non-PEGylated GNP robustly inhibited uptake of TMR-dextran as visualized by fluorescence microscopy, surface-passivated PEGylated GNP had no effect on the uptake of TMR-dextran (Figure 3e). Quantification of dextran uptake further revealed a robust inhibition of macropinocytosis by non-PEGylated GNP (Figure 3f), while PEGylated GNP caused no inhibition, further confirming that the GNP surface plays a crucial role.

All of the above results indicate that interactions of nonmodified GNP with RAS are playing a critical role to inhibit RAS activation. To address this question further, we investigated whether GNP could pull down KRAS in the biomolecular corona around PEGylated and non-PEGylated GNP. As proof-of-principle studies, we prepared cellular lysates from PANC-1, BXPC-3, and OVCAR-4 cells, incubated them separately with PEGylated and non-PEGylated GNP, pulled down by centrifugation, and purified by washing with deionized water once (represented as the scheme in Figure 3g). The resulting protein corona samples of non-PEGylated and PEGylated GNP were characterized using UV−visible spectroscopy (Figure S6a) followed by measuring hydrodynamic size and zeta potentials (Table S1). As expected, for non-PEGylated GNP, hydrodynamic size was increased to 35.56 nm and zeta potential was changed to −21.0 mV (Figure

https://doi.org/10.1021/acsnano.3c00920
ACS Nano XXXX, XXX, XXX−XXX

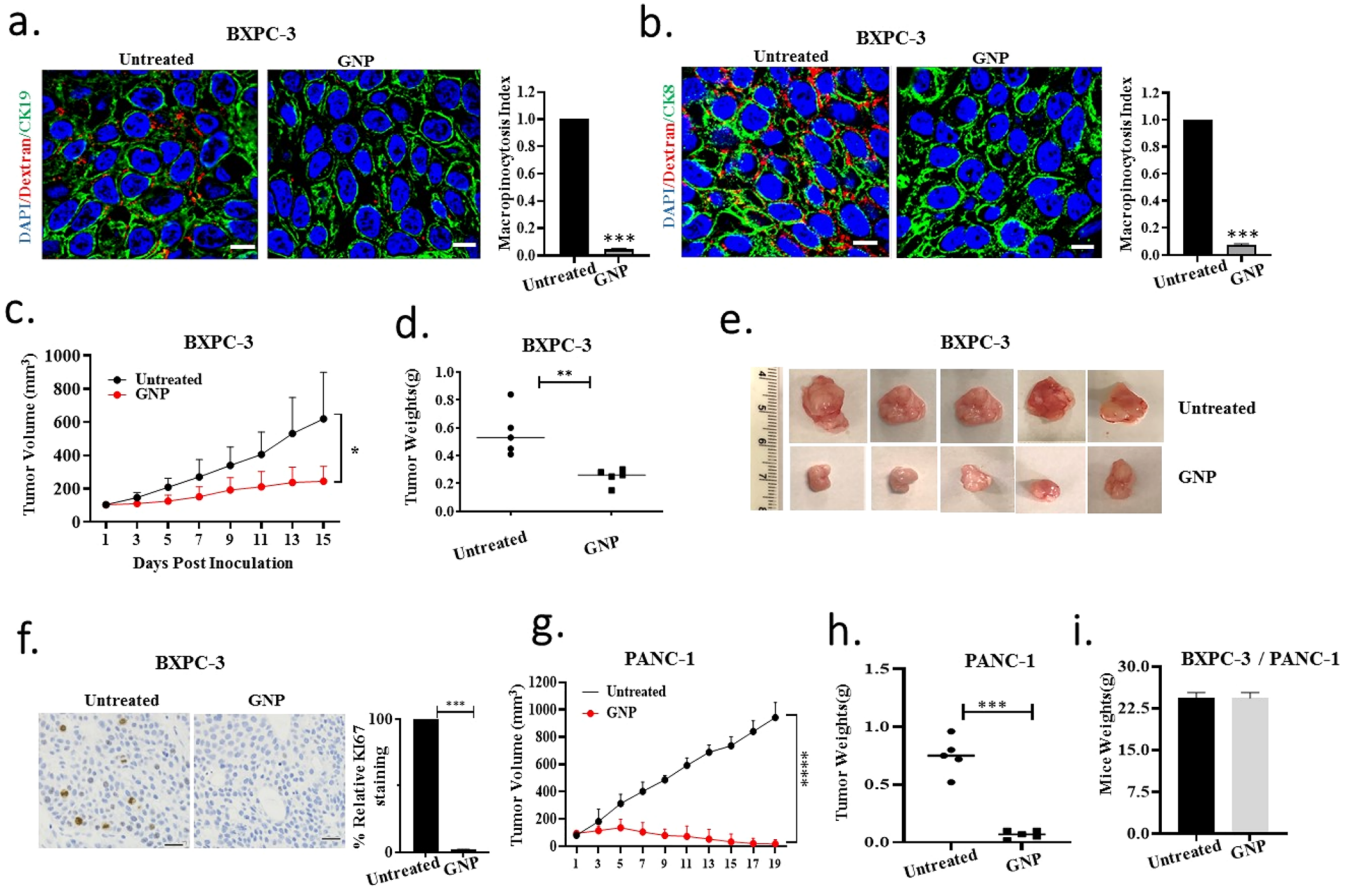

Figure 4. GNP treatments inhibit tumor macropinocytosis phenotype and tumor burden *in vivo*. (a) Macropinocytosis inhibition property of GNP in *vivo* was confirmed by TMR-dextran uptake inhibition in GNP-pretreated mouse tumors. Briefly, mice were subcutaneously implanted with 5×10^6 BXPC-3 cells, and tumors were allowed to grow to 400 mm^3. Mice then received intravenous administration of 200 μg of GNP every other day for a total of three doses. Mice were then anesthetized, and TMR-dextran 1 mg/tumor/mouse was intratumorally injected in 5 or 6 locations. After 60 min, mice were euthanized and dextran-treated tumors were collected and submitted for sectioning. Cell boundaries in sections were stained with either CK-8 or CK-19 along with DAPI staining for nuclei, and macropinosomes were visualized using a confocal microscope; scale bar = 20 μm. Quantification of dextran represented in right panels using ImageJ software. ***$P < 0.001$. (c) Tumor regression efficacy of intravenously administered GNP in mice implanted with 5×10^6 BXPC-3 cells in the subcutaneous model. Post tumor implantation, when the tumor size reached 100 mm^3, 200 μg of GNP was administered every other day for eight injections. (d) Average tumor weights and (e) digital image of BXPC-3 tumors obtained from untreated and GNP-treated mice after final administration of GNP. (f) Relative tumor proliferative inhibition efficacy of GNP in treated BXPC-3 tumors using proliferative marker Ki67 staining. Scale bar represents 10 μm. (g) Tumor regression efficacy of intravenously administered GNP in mice implanted with 5×10^6 PANC-1 cells in a subcutaneous model. After tumor implantation, when the tumor size reached 100 mm^3, 200 μg of GNP was administered every other day for eight injections. (h) Average tumor weights obtained on the termination day of experiment. (i) Average weights obtained from untreated or GNP-treated mice implanted with either BXPC-3 or PANC-1 cells after completion of GNP administrations. Mean ± SD, ***$P < 0.001$.

S5b), which confirmed bimolecular protein layer formation around the GNP. These physicochemical analyses showed similar trends when compared with their corresponding non-PEGylated protein corona samples (Table S1). Next, equal amounts of protein were probed for KRAS expression by immunoblot analysis. Immunoblot analyses revealed that KRAS was present in the biomolecular corona from BXPC-3, PANC-1, and OVCAR-4 cells as well as in their respective supernatant (Figure 3g). Importantly, surface passivation of GNP by PEGylation abolished the ability of GNP to pull down KRAS, and KRAS was found only in the supernatant and not in the biomolecular corona around PEGylated GNP (Figure 3h). Interestingly, loading controls such as GAPDH, α-tubulin, and β-actin were not present in the biomolecular corona around 20 nm GNP, suggesting specificity of GNP toward KRAS, although the mechanism of such specificity is currently unknown (Figure 3h). Since KRAS mutation is near ubiquitous in PDAC, we next investigated the ability of GNP to sequester KRAS mutants such as G12D or K147L.[25] We introduced HA-tagged wild-type KRAS (HA-WT-KRAS), G12D (HA-G12D-KRAS), and Flag-tagged K147L (Flag-K147L-KRAS) in human embryonic kidney (HEK) fibroblast cells (Figure S7), followed by cellular lysis and biomolecular corona formation as described above. The presence of KRAS in the biomolecular corona as well in the supernatant was probed by immunoblotting against, HA, Flag, and KRAS. Immunoblot analysis revealed that wild-type and mutant KRAS were present in the bimolecular corona around GNP (Figure 3i). All of these results taken together suggest that the unmodified GNP surface plays a crucial role in sequestering both wild-type and mutant KRAS proteins, leading to inhibition of KRAS activation, macropinocytosis, and cancer cell proliferation.

https://doi.org/10.1021/acsnano.3c00920
ACS Nano XXXX, XXX, XXX−XXX

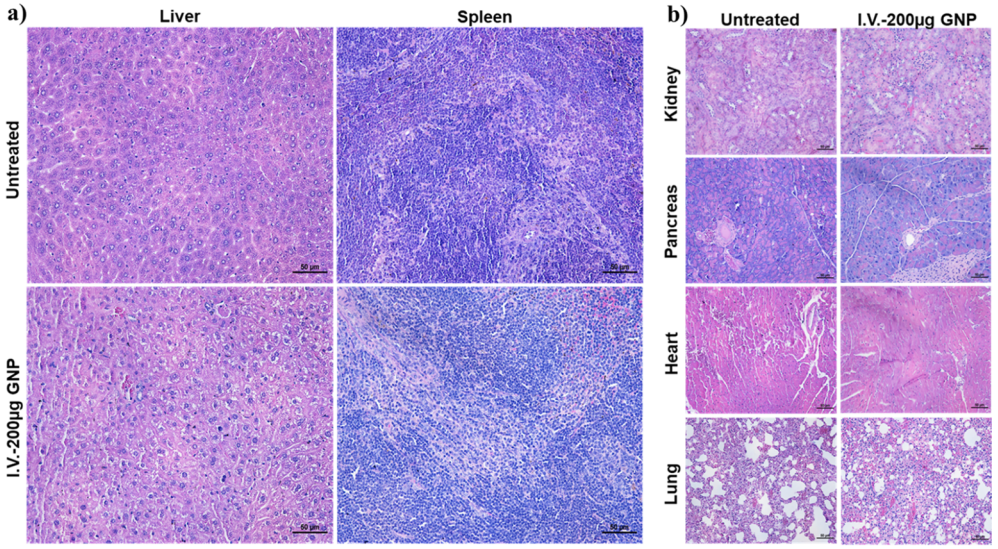

Figure 5. Histopathological analysis for the evaluation of toxicities induced by GNP in a PANC-1 *in vivo* model. (a, b) Histological analyses. H&E-stained tissue sections from untreated mice and mice treated with 200 μg of GNP given intravenously. (a) Liver and spleen representative images for untreated and 200 μg GNP-treated animals. (b) Kidney, pancreas, heart, and lung representative images from the same animals for untreated and 200 μg GNP-treated animals. Images of all whole-sectioned tissues were captured by a Nikon microscope. Scale bar, 50 μm.

Impact of GNP on Macropinocytosis and Tumor Growth *in Vivo*. Next we investigated the impact of GNP treatment in inhibiting macropinocytosis and tumor growth *in vivo*. We used subcutaneous human xenograft models as reported previously by implanting BXPC-3 cells in 6−8-week-old female nude mice.[17,19] To rule out the influence of tumor size on the *in vivo* macropinocytosis study, tumors were allowed to grow to ∼400 mm^3 size before dividing the mice into control and GNP treatment groups. While animals in the control group were left untreated, the GNP treatment group received only 3 doses of GNP (200 μg/animal) via intravenous injection to avoid the inhibition of tumor growth by GNP. The dosage of GNP of 200 μg/mouse was determined based on our previous reports that this dose, in comparison to 100 and 400 μg/mouse, achieved the best therapeutic effect against A2780 and SKOV3 orthotopic tumors.[14] This dosage also resulted in higher GNP uptake into tumors. Despite significant uptake by the liver and marginal uptake by the lungs and kidneys, no sign of toxicity to the animals was observed.[14] We have also previously reported that GNP 200 μg/mouse inhibited tumor growth in an orthotopic co-implantation model of pancreatic cancer.[16]

Furthermore, we recently compared the biodistribution of GNP of 20 nm size in normal mice following two routes of administration that are commonly used in the treatment of cancer, i.e., the intravenous (i.v.) and intraperitoneal (i.p.) routes. We also compared a range of GNP doses, given either as a single dose or as multiple doses over 2 weeks. Since the bioaccumulation of GNP may be associated with toxicities *in vivo*, we first determined the biodistribution of injected GNP in various body tissues to assess both dose-related toxicities and the effect of the route of administration. For this, normal mice received GNP by either i.v. or i.p. injection (100−300 μg per mouse) in either an acute setting (24 h and single injection of GNP) or a chronic setting (GNP injections every 2 days for 14 days). Importantly, biochemical and immunohistochemical analyses revealed the absence of toxicity.[23] In the present study, three doses of GNP treatment did not appreciably reduce the tumor size. Herein, prior to euthanizing mice, TMR-dextran was intratumorally injected (5−6 locations/tumor); tumor tissues were processed and dextran uptake was determined by fluorescence microscopy. Fluorescence images revealed that GNP treatment robustly inhibited dextran uptake in tumor when compared with control tumors of comparable size, confirming inhibition of macropinocytosis by GNP *in vivo* (Figure 4a and 4b). Cell boundaries in the tumor tissue sections were stained with either anti-CK-8 antibody or anti-CK-19 antibody. We next, investigated the impact of GNP treatment on tumor growth in two separate human xenograft models of pancreatic cancer. In separate groups of animals BXPC-3 (harboring wild-type KRAS) and PANC-1 (harboring mutant KRAS) cells were implanted subcutaneously and mice divided into control and GNP-treatment groups when the tumors reached ∼100 mm^3 in size. Tumor growth was monitored over time using slide calipers. Monitoring tumor growth over time revealed that 200 μg GNP/injection/mouse treatment significantly inhibited tumor growth in both models (Figure 4c to g). Tumor growth inhibition by GNP treatment was further confirmed by significant reduction in tumor mass in both the models (Figure 4d, e, and h). Analyses of tumor cell proliferation by staining with Ki67 in tumor sections revealed a significant reduction in the number of proliferative cells (Figure 4f) in the GNP-treated groups when compared with the animals in the control groups. Furthermore, there are no appreciable changes in body weights, indicative of lack of toxicity due to GNP treatment (Figure 4i). Summarizing all the results, it becomes clear that unmodified GNP inhibits macropinocytosis and tumor growth by decreasing KRAS activation, and the GNP surface plays a crucial role. Moreover, since PANC-1 cells are RAS mutated while BXPC-3 cells have wild-type RAS, it may be possible that GNP inhibit tumors from RAS-mutated cells more effectively than RAS wild-type cells. The impact of GNP on cells harboring mutant RAS compared to wild-type RAS is a part of our future investigation and is beyond the scope of the present paper.

https://doi.org/10.1021/acsnano.3c00920
ACS Nano XXXX, XXX, XXX−XXX

Evaluation of Toxicities Induced by GNP. To evaluate the toxicity induced by GNP, we performed immunohistochemistry profiles following GNP treatment in the PANC-1 *in vivo* mouse model, the therapeutic study (Figure 5) and immunohistochemical analyses to evaluate GNP-induced toxicities in the mice receiving 200 μg of GNP given intravenously in the macropinocytosis study (Figure S8). Immunohistochemical analyses were performed in normal tissues including the liver, spleen, kidney, pancreas, heart, and lung. The results demonstrate that there was no significant morphological difference between the GNP-treated and untreated groups. Importantly, there was no change in body weights of untreated and GNP-treated mice throughout the experiment. Collectively, these results suggest that GNP are nontoxic to normal tissues.

CONCLUSIONS

PDAC is a devastating disease with dismal prognosis where mutations in the *KRAS* gene are near ubiquitous (>95%).[26,27] As well as activating a series of proliferative signaling cascades, mutations in *RAS* genes importantly provide metabolic adaptation to the tumor cells to supply essential building blocks to support growth and survival. While macropinocytosis is a metabolic adaptation used by diverse cell types to maintain normal cellular homeostasis, it is aberrantly activated by RAS-transformed cancer cells.[28,29] Therefore, careful interrogation of macropinocytosis is warranted to inhibit PDAC growth and mitigate any side effects.

The ability of GNP to inhibit HB-GFs has shown promise to inhibit tumor growth, metastasis, and therapy resistance in a number of cancers.[14,23,30] GNP have also been used as a therapeutic molecule in a number of noncancerous diseases including rheumatoid arthritis, diseases of the eye, and neurodegenerative diseases such as Alzheimer's disease.[31−34] However, the ability of GNP to modulate KRAS activation and macropinocytosis has not yet been tested. Our finding of GNP-mediated inhibition of macropinocytosis and tumor growth in two independent preclinical models of PDAC demonstrates its potential utility to inhibit tumor growth in other malignancies harboring RAS mutations.

The current finding that GNP inhibit activation of both wild-type and mutant KRAS is interesting and may be exploited to inhibit macropinocytosis in other RAS-transformed cancer cells apart from PDAC. This inhibition is independent of involvement of the RAS regulators, RAS-GAP and RAS-GEF. Interestingly, characterization of the biomolecular corona around GNP through immunoblot assays confirms that the unmodified GNP surface is critical to sequester both wild-type and mutant RAS and decrease its activation. PEGylation of the NP surface to confer NP with stealth properties is well established in the nanomedicine community.[35] PEGylation prevents adsorption of opsonins to the NP surface, thereby preventing their clearance via opsonization.[36] Reducing protein adsorption by PEGylation may be preventing RAS binding to PEGylated GNP. The results from EGF stimulation demonstrate that the inhibition of KRAS activation by GNP is independent of growth factor stimulation. Collectively, our data demonstrate that GNP have an ability to sequester and decrease activation of both wild-type and mutant RAS, irrespective of growth factor signaling. The presence of KRAS, both mutant and wild type, in the biomolecular corona does not preclude indirect binding through protein complexes. Interestingly, the absence of abundant cellular proteins used as loading controls such as tubulin, GAPDH, and β-actin indicates affinity of GNP toward RAS or RAS-binding proteins. Such affinity may depend on the overall charge of the proteins, similar to the ability of GNP to bind HB-domain-containing proteins. As shown in Figure 1c, synthesized GNP without PEGylation exhibit a negative zeta potential value, correlating with a negatively charged surface of the NP.[37] KRAS proteins have been shown to favor interaction with negatively charged surfaces, such as cell membranes,[38] demonstrating a possible indication of high-affinity interactions between synthesized GNP and KRAS based on favorable electrostatics. This phenomenon could also explain why synthesized GNP do not exhibit interaction with protein-loaded controls. Tubulin, GAPDH, and β-actin possess negative charges that would repel synthesized GNP and limit binding affinity.[39] Recently, the biomolecular corona around GNP has also been used as a nonconventional way to identify critical molecules responsible for tumor growth and therapy resistance.[40] Mass spectrometric characterization of the biomolecular corona around 5 nm GNP, either completely or partially protected by cetuximab (C225), recently led to the identification of UBAP2 as a regulator of KRAS activation and macropinocytosis in PDAC.[19,41] Therefore, identification of biomolecular corona components around GNP from pancreatic cancer specimens (serum/plasma, tissues lysates) may provide translational opportunities to modulate RAS activation, macropinocytosis, and tumor growth.

METHODS

i. Synthesis and Characterization of GNP. GNP were synthesized by the citrate reduction method using gold chloride ($HAuCl_4 \cdot 3H_2O$) solution as a precursor for GNP following our previously established protocol.[14,42] Briefly, 500 μL of 100 mM gold chloride stock solution was diluted into 155 mL of endotoxin-free water (G-Biosciences, St. Louis, MO, USA) and heated at 340 °C until boiling started. To this boiling solution was added 45 mL of 1% sodium citrate solution, and the solution was stirred for another 10 to 15 min until the color of the solution turned to wine red. The solution was then moved to room temperature and stirred at room temperature overnight. Synthesized GNP were characterized using UV−visible spectroscopy (Spectrostar Nano, BMG Labtech), measuring hydrodynamic size (DLS) and zeta potentials using a Nano ZS, Malvern Zetasizer instrument, equipped with a laser wavelength of 633 nm, and TEM using a JEOL 2000-FX instrument.

ii. Cell Culture Media. BXPC-3, AsPC-1, OV-90, and OVCAR-4 cells were cultured in RPMI, and PANC-1 cells were cultured in DMEM medium. Media was supplemented with 10% heat-inactivated fetal bovine serum (FBS) (Gibco, Grand Island, NY, USA) and 100 units of penicillin and 100 μg of streptomycin per mL (Invitrogen, Rockford, IL, USA) in a 5% CO_2 humidified atmosphere.

iii. Macropinocytosis Assay. Visualization and quantification of macropinosomes in cells was performed according to the protocol established by Commisso et al. with slight modifications.[1,17] Briefly, after seeding 0.1×10^6 cells on coverslips in 12-well plates, they were allowed to grow in the incubator for 24 h. The next day, media was replaced with serum-free media, and cells were maintained in serum-free media for another 24 h followed by treatment with 25 μg/mL of 20 nm GNP for 48 h or left as untreated controls in serum-free media. After 48 h of treatment, cells were washed thrice with ice-cold PBS, followed by addition of 1 mg/mL TMR-dextran (MW 70 kDa, Invitrogen) in serum-free media to both GNP-treated and control groups and incubation for an additional 1 h at 37 °C. Cells were then washed thoroughly (5 × PBS washings) followed by fixation with 4% formalin solution. For macropinocytosis assays in NIH3T3 cells, briefly, 1.5×10^5 cells were seeded in 12-well plates and allowed to grow for 24 h in complete media. The next day, the media was

https://doi.org/10.1021/acsnano.3c00920
ACS Nano XXXX, XXX, XXX−XXX

replaced with serum-free media and cells were incubated with 25 μg/mL of 20 nm GNP or untreated as a control for another 24 h. After 24 h of treatment, cells were washed thrice with ice-cold PBS followed by the addition of 1 mg/mL TMR-dextran in serum-free media to both GNP-treated and control groups and incubated for an additional 1 h at 37 °C. Cells were then washed thoroughly (5 × PBS) followed by fixation with 4% formalin solution. Finally, cells were mounted with DAPI-containing mounting media, and slides were prepared to visualize under fluorescence microscopy. Dextran-TMR uptake in cells was captured using an Axiovert 200 inverted fluorescent microscope, and resulting TMR- and DAPI-stained areas were analyzed by ImageJ software (National Institutes of Health) using the analyze particles feature. Dextran uptake assays in each cell line were repeated at least three times, and images from 5 to 10 random fields of each prepared slide were obtained. Macropinocytotic index (MI) was calculated using the formula $(\mathrm{AREA}_{\mathrm{DEXTRAN}} \div \mathrm{AREA}_{\mathrm{CELLS}}) \times 100\%$. Obtained results after quantification were represented as relative dextran uptake by normalizing the untreated control group as 1.0.[17]

iv. Comparison of the Effects of GNP and EIPA (a Small Molecular Inhibitor of Macropinocytosis). To compare GNP to the macropinocytotic inhibitor EIPA, PANC-1 cells were seeded on coverslips and were allowed to grow in the incubator for 24 h. The next day, media was replaced with serum-free media and cells were maintained in serum-free media for another 24 h. For the GNP treatment group, cells were treated with 25 μg/mL of 20 nm GNP for 48 h or left untreated as controls in serum-free media. After 48 h of treatment, cells were washed thrice with ice-cold PBS followed by addition of 1 mg/mL TMR-dextran in serum-free media to both GNP-treated and control groups and incubated for an additional 1 h at 37 °C. For EIPA, as a positive control inhibiting macropinocytosis, treatment, media was replaced with serum-free media and kept in an incubator for another 72 h. After that, cells were incubated with 75 μM EIPA for 2 h followed by addition of 1 mg/mL TMR-dextran for 1 h at 37 °C. Cells were then washed thoroughly (5 × PBS) followed by fixation with 4% formalin solution. Finally, cells were mounted with DAPI-containing mounting media, and slides were prepared to visualize under fluorescence microscopy.

v. Macropinosome Colocalization with Lysosome Experiment. Macropinosome localization with lysosomes was performed following the protocol of the TMR-dextran uptake experiment but using BSA-Alexa Fluor-488 (Invitrogen) instead followed by lysosome staining using Lysotracker Red DND-99 (Invitrogen). Briefly, after seeding, starvation, and GNP treatment cells were incubated for 1 h with BSA-Alexa Fluor 488 and analyzed as described above. After washing with ice-cold PBS, Lysotracker DND-99 was added and incubated for 30 min followed by multiple washing steps with ice-cold PBS (5 times). Finally, cells were fixed with 4% formalin solution and mounted with DAPI-containing mounting media, and slides were prepared to visualize by fluorescence as described above.

vi. Transferrin Uptake Experiments. Transferrin uptake experiments were performed using Alexa Fluor-488-conjugated transferrin. Briefly, cells were treated with GNP for 48 h or left as untreated controls as described above. After 48 h cells were supplemented with 25 mM HEPES pH 7.4 and 0.5% BSA and incubated for 30 min. Then 50 μg/mL of Alexa Fluor-488-conjugated transferrin was added and incubated for an additional 40 min. Following extensive washings with ice-cold PBS, cells were fixed with 4% formaldehyde solution and mounted on slides using mounting media with DAPI (Vector). For the positive control, cells were treated with 40 μM chlorpromazine instead of GNP and processed for visualization by a fluorescence microscope as described above. Results were analyzed from the florescence images taken from the untreated, GNP-treated, and chrolopromazine-treated cells.

vii. Small GTPase Pull-Down Assay. Amounts of GTP binding to small GTPases were evaluated using the RAS activation assay kit (Cytoskeleton Inc., Denver, CO, USA, Cat. # BK008) following the manufacturer's protocol. Briefly, cells (0.7×10^6) were seeded in 10 cm dishes and allowed to grow in their respective serum-containing media for 24 h. After 24 h, cell culture media were replaced with the respective serum-free media, and cells were maintained in serum-free media for an additional 24 h. After 24 h, cells were either treated with 25 μg/mL of GNP for 48 h or left as untreated control. After 48 h of treatment, all cells were washed three times with ice-cold PBS and lysed according to the manufacturer's protocol. The clarified lysates were then incubated with GST-Raf-RBD (for RAS) and immobilized on glutathione−agarose beads (30 μL beads) with 500 μg of cell lysate for 1 h at 4 °C. The amount of GTP-bound RAS content and total RAS was determined by Western blotting using an antibody against RAS (Cat: ab-52939).

viii. RAS Downstream Signaling. To check the effect of 20 nm GNP on the RAS downstream signaling network in PANC-1 cells, 1×10^6 cells were seeded in a 10 cm dish and incubated for 24 h followed by starvation for another 24 h, after replacing with starvation medium (DMEM without 10% FBS). The next day, cells were either treated with GNP at 25 μg/mL or left untreated and incubated for 48 h. Cells were washed thrice with ice-cold PBS, and lysates were collected to see the change in expression of downstream proteins involved in RAS signaling using Western blotting.

ix. Toxicity Effect of GNP. The proliferation inhibition effect of GNP in cells after treatment was determined using manual counting. Briefly, 0.75×10^6 PANC-1, BXPC-3, OVACAR-4, AsPC-1, and OV-90 cells were seeded in 100 mm dishes and allowed to grow in the incubator for 24 h. The next day, the media was replaced with corresponding starvation medium and allowed to incubate for 24 h followed by treatment with freshly prepared GNP at 25 μg/mL for 48 h or left as untreated. After 48 h, cells were washed thrice with ice-cold PBS and trypsinized to obtain a cell pellet. Cell count in the pellet suspension was done manually on a hemocytometer.

x. PEGylation of GNP. PEGylation of GNP was done by addition of methoxy-PEG (1000)-SH to freshly prepared bare 20 nm GNP. Briefly, 1, 2, 3, 4, 5, 7.5, or 10 μg of methoxy-PEG (1000)-SH in 1 mL of water was added to GNP (50 μg/mL solution) and stirred for 1 h at room temperature. NP surface saturation after PEGylation was validated by addition of 150 mM NaCl solution, which generally results in particle aggregation due to the bare surface or partial surface coverage with PEG molecules. After synthesis, physicochemical characterization was performed by measuring UV-absorption spectra, DLS size (nm), and zeta potential (ζ). Concentrated PEGylated GNP were collected as pellets using centrifugation at 10 000 rpm for 20 min, and the concentration of NP in the pellet was measured based on absorbance.

xi. Nanoparticle−Protein Corona (NP-PC) Preparation and Characterization. The protein corona around GNP was prepared using our previously published protocol.[13] Briefly, 200 μg of cell lysates prepared from PANC-1, OVCAR-4, or BXPC-3 cells was mixed with 50 μg of either freshly prepared GNP or PEGylated GNP in Eppendorf tubes and incubated on an end-over-end rotator for 18 h at room temperature. The next day, physicochemical characterization studies of NP-PCs were performed using DLS and zeta potential (ζ) measurements to confirm the protein corona formation around the GNP. NP-PCs were isolated as NP pellets using centrifugation at 10 000 rpm for 20 min at 4 °C. Resulting pellets were washed at least twice using deionized water to separate unbound or partially bound proteins. The BCA assay was used to measure the amount of protein adsorbed on GNP surfaces as well as protein in corresponding supernatants.

xii. Western Blot Analysis of NP-PCs. Pulldown of KRAS protein by GNP from the lysates after incubation was validated using Western blot analysis of NP-PCs samples. Briefly, 10 μg of protein lysates, NP-PCs, and PEGylated NP-PCs along with their corresponding supernatants obtained after centrifugation were loaded in 12% gels and run for analysis. After transfer to the PVDF membrane, KRAS protein on membranes was detected using KRAS primary antibody (Protein Tech, Cat. 12063-1-AP) followed by corresponding secondary HRP-conjugated antibody.

xiii. Expressing KRAS Mutants in Cells. A total of 1×10^6 HEK-293 cells were individually transfected with 2 μg of HA-WT-KRAS (Addgene, Watertown, MA, USA), HA-G12D-KRAS (Addgene), and Flag-K147L-KRAS plasmids (kind gift from Atsuo T. Sasaki,

https://doi.org/10.1021/acsnano.3c00920
ACS Nano XXXX, XXX, XXX−XXX

Department of Medicine, Harvard Medical School, Boston, MA, USA) using FuGENE 6 transfecting reagent. After 48 h of transfection, lysates were collected and Western blot analyses were performed to determine the successful transfection. Expression of mutants WT-KRAS, G12D-KRAS, and K147L-KRAS was confirmed by blotting the membrane against their corresponding HA or FLAG tags and KRAS antibodies.

xiv. Protein-Corona Studies Using RAS Mutants. GNP specificity toward particular KRAS mutations was determined by incubating GNP with lysates of HEK-293 cells pretransfected with KRAS mutants followed by the Western blot analysis of the samples using the protocol described earlier. Briefly, following separate WT-KRAS, G12D-KRAS, and K147L-KRAS transfections in HEK-293 cells, lysates were prepared, and 200 μg of each lysate was incubated separately with 50 μg of GNP on an end-over-end rotator for 18 h at room temperature. The next day, NP-PCs were separated as pellets using centrifugation as previously described. After BCA assays, 10 μg of protein lysates, GNP-PCs, and corresponding supernatants were loaded on 12% gels for Western blot analysis to determine the presence of KRAS mutants. Membranes were blotted with corresponding primary HA or FLAG tags or KRAS antibodies followed by blotting with secondary antibodies.

xv. Macropinocytosis Inhibition *in Vivo*. *In vivo* macropinocytosis inhibition efficacy of GNP was tested in mice subcutaneously implanted with BXPC-3 tumors in which macropinosomes were stained with TMR-dextran. Briefly, athymic Ncr-nu female nude mice were housed and kept under pathogen-free conditions following American Association of Accreditation of Laboratory Animal Care guidelines. A total of 2×10^6 BXPC-3 cells in 1:1 dilution with Matrigel (BD Biosciences) were implanted subcutaneously in a total of 10 mice (5 mice for the untreated and 5 animals for the 20 nm GNP treatment group), and after implantation tumor growth over time was monitored using Vernier calipers. Four weeks after implantation, when tumors reached an average volume of 400 mm^3, for the GNP-treated group 200 μg of GNP per mouse per dose was intravenously injected every other day for a total three doses. On the following day, mice were anesthetized using ketamine and xylazine, and 1 mg of TMR-dextran in 100 μL of PBS per tumor was slowly administered intratumorally. After 60 min, mice were euthanized and tumors were collected, frozen in OCT media (Tissue-Tek, Torrance, CA, USA), and submitted for section preparation on slides. For untreated tumor section controls, tumors from nontreatment group mice with similar tumor sizes (~400 mm^3) were injected with TMR-dextran and processed. Cell boundaries in *in vivo* tumor sections were stained either with anti-CK-8 antibody (to stain the fresh transplanted epithelial cells) or with anti-CK-19 antibody (to stain the acinar cells) in tumors. Macropinosome visualization in tumor sections of slides was done by using an Olympus FV1000 confocal microscope using either a 60× or 100× lens in 5 to 10 random fields in sections, and the TMR-dextran florescence was quantified using ImageJ software as discussed in *in vitro* studies. All experimental *in vivo* studies were performed according to the protocol approved by the Institutional Animal Care and Use Committee (IACUC) at the University of Oklahoma Health Sciences Center.

xvi. Tumor Regression Studies *in Vivo*. *In vivo* tumor regression efficacy of GNP was validated in mice subcutaneously implanted with BXPC-3 or PANC-1 tumor cells. Briefly, 5×10^6 of either BXPC-3 or PANC-1 cells were injected subcutaneously in a total of 20 athymic Ncr-nu female mice and tumors allowed to develop. When tumor size reached 100 mm^3, mice were separated into untreated and GNP-treated groups containing 5 mice per group for both BXPC-3 and PANC-1. Each mouse in the treated group was administrated 200 μg of GNP intravenously every other day, and the control mice were left as untreated controls. After careful monitoring for 21 days, mice were euthanized and tumors along with organs were collected for further analysis.

xvii. Statistical Analysis. All experiments reported here were repeated at least three times unless stated, and error bars represent mean values ± SD. Statistically significant differences between untreated and GNP treatment groups were evaluated by either two-way ANOVA software in GraphPad Prism version 8.4.3 or using two-sided Student's *t* test. *P* value ≤ 0.05 was considered as statistically significant.

ASSOCIATED CONTENT

Supporting Information

The Supporting Information is available free of charge at https://pubs.acs.org/doi/10.1021/acsnano.3c00920.

Fluorescence images of GNP inhibition of lysosomal localization; fluorescence images GNP inhibition compared with transferrin; GNP effects on RAS regulators; absorbance spectra of PEGylated GNP; size, zeta potentials, and TEM images of GNP-PEG; absorbance spectra of protein corona coated GNP; KRAS mutant expressions in HEK; GNP toxicity analysis of H&E images *in vivo*; GNP compared with amiloride effects on macropinocytosis; macropinocytosis in NIH3T3 (PDF)

AUTHOR INFORMATION

Corresponding Author

Priyabrata Mukherjee − *Department of Pathology, University of Oklahoma Health Sciences Center, Oklahoma City, Oklahoma 73104, United States; Peggy and Charles Stephenson Cancer Center, University of Oklahoma Health Sciences Center, Oklahoma City, Oklahoma 73104, United States;* orcid.org/0000-0002-0557-0833; Phone: 405-271-1133; Email: Priyabrata-Mukherjee@ouhsc.edu

Authors

Chandra Kumar Elechalawar − *Department of Pathology, University of Oklahoma Health Sciences Center, Oklahoma City, Oklahoma 73104, United States*

Geeta Rao − *Department of Pathology, University of Oklahoma Health Sciences Center, Oklahoma City, Oklahoma 73104, United States*

Suresh Kumar Gulla − *Department of Pathology, University of Oklahoma Health Sciences Center, Oklahoma City, Oklahoma 73104, United States*

Maulin Mukeshchandra Patel − *Department of Cell Biology, University of Oklahoma Health Sciences Center, Oklahoma City, Oklahoma 73104, United States*

Alex Frickenstein − *Stephenson School of Biomedical Engineering, University of Oklahoma, Norman, Oklahoma 73019, United States*

Nicolas Means − *Department of Pathology, University of Oklahoma Health Sciences Center, Oklahoma City, Oklahoma 73104, United States*

Ram Vinod Roy − *Department of Pathology, University of Oklahoma Health Sciences Center, Oklahoma City, Oklahoma 73104, United States*

Leonidas Tsiokas − *Department of Cell Biology, University of Oklahoma Health Sciences Center, Oklahoma City, Oklahoma 73104, United States*

Sima Asfa − *Department of Pathology, University of Oklahoma Health Sciences Center, Oklahoma City, Oklahoma 73104, United States*

Prasanta Panja − *Department of Pathology, University of Oklahoma Health Sciences Center, Oklahoma City, Oklahoma 73104, United States*

Chinthalapally Rao − *Center for Cancer Prevention and Drug Development, Department of Medicine, Stephenson Cancer*

https://doi.org/10.1021/acsnano.3c00920
ACS Nano XXXX, XXX, XXX−XXX

Center, University of Oklahoma Health Sciences Center, Oklahoma City, Oklahoma 73104, United States

Stefan Wilhelm − *Stephenson School of Biomedical Engineering, University of Oklahoma, Norman, Oklahoma 73019, United States*

Resham Bhattacharya − *Department of Obstetrics and Gynecology, University of Oklahoma Health Sciences Center, Oklahoma City, Oklahoma 73104, United States*

Complete contact information is available at: https://pubs.acs.org/10.1021/acsnano.3c00920

Author Contributions

C.K.E. and G.R. have equally contributed to the research. S.K.G. has performed the tumor regression studies. M.P. helped in confocal imaging of dextran tumor slides. S.A. has done CK-8 and CK-19 labeling in tumor sections. P.P. helped with NIH3T3 macropinocytosis studies, and C.R. helped in toxicity studies. The research was conceived, designed, and supervised by P.M. R.B. was involved in conceptualization and scientific discussions. A.F. has done the TEM imaging of PEGylated GNP.

Funding

This work was supported by National Institute of Health Grants CA220237, CA136494, CA213278, CA253391, and CA260449-01A1 (to P.M). S.W. acknowledges NIH COBRE (P20GM135009) and NSF CAREER (2048130) for funding. P.M. also acknowledges the Institutional Development Award (IDeA) of NIH under grant no. P20GM103639.

Notes

The authors declare no competing financial interest.

ACKNOWLEDGMENTS

We thank the Peggy and Charles Stephenson Cancer Center at the University of Oklahoma Health Sciences Center for a seed grant and an Institutional Development Award (IDeA) from the National Institute of General Medical Sciences of the National Institutes of Health under grant number P20 GM103639. Research reported in this publication was also supported in part by the National Cancer Institute Cancer Center Support Grant P30CA225520 and the Oklahoma Tobacco Settlement Endowment Trust contract awarded to the University of Oklahoma Stephenson Cancer Center. P.M. also acknowledges Peggy and Charles Stephenson Endowed Chair for Laboratory Cancer Research Fund to partly support this work. We thank all authors involved in this research and who participated in scientific discussion. S.W. and A.F. acknowledge the assistance of Dr. Preston Larson and Dr. Julian Sabisch and additionally the University of Oklahoma (OU) Samuel Roberts Noble Microscopy Laboratory (SRNML). We also thank Peggy and Charles Stephenson Cancer Center at University of Oklahoma Health Sciences Center for a seed grand and Institutional Development Award (IDeA) of NIH under grant no. P20GM103639 for Histology and Immunohistochemistry Core for the use of immunohistochemistry core and imaging.

REFERENCES

(1) Commisso, C.; Davidson, S. M.; Soydaner-Azeloglu, R. G.; Parker, S. J.; Kamphorst, J. J.; Hackett, S.; Grabocka, E.; Nofal, M.; Drebin, J. A.; Thompson, C. B.; et al. Macropinocytosis of protein is an amino acid supply route in Ras-transformed cells. *Nature* **2013**, *497*, 633−637.

(2) Jayashankar, V.; Edinger, A. L. Macropinocytosis confers resistance to therapies targeting cancer anabolism. *Nat. Commun.* **2020**, *11*, 1121.

(3) Swanson, J. A. Shaping cups into phagosomes and macropinosomes. *Nat. Rev. Mol. Cell Biol.* **2008**, *9*, 639−649.

(4) Bloomfield, G.; Kay, R. R. Uses and abuses of macropinocytosis. *J. Cell Sci.* **2016**, *129*, 2697−2705.

(5) Mercer, J.; Helenius, A. Virus entry by macropinocytosis. *Nat. Cell Biol.* **2009**, *11*, 510−520.

(6) Bar-Sagi, D.; Feramisco, J. R. Induction of membrane ruffling and fluid-phase pinocytosis in quiescent fibroblasts by ras proteins. *Science* **1986**, *233*, 1061−1068.

(7) Zhang, Y.; Recouvreux, M. V.; Jung, M.; Galenkamp, K. M. O.; Li, Y.; Zagnitko, O.; Scott, D. A.; Lowy, A. M.; Commisso, C. Macropinocytosis in Cancer-Associated Fibroblasts Is Dependent on CaMKK2/ARHGEF2 Signaling and Functions to Support Tumor and Stromal Cell Fitness. *Cancer Discov* **2021**, *11*, 1808−1825.

(8) Zhang, Y.; Elechalawar, C. K.; Hossen, M. N.; Francek, E. R.; Dey, A.; Wilhelm, S.; Bhattacharya, R.; Mukherjee, P. Gold nanoparticles inhibit activation of cancer-associated fibroblasts by disrupting communication from tumor and microenvironmental cells. *Bioact Mater.* **2021**, *6*, 326−332.

(9) Sasaki, A. T.; Carracedo, A.; Locasale, J. W.; Anastasiou, D.; Takeuchi, K.; Kahoud, E. R.; Haviv, S.; Asara, J. M.; Pandolfi, P. P.; Cantley, L. C. Ubiquitination of K-Ras enhances activation and facilitates binding to select downstream effectors. *Sci. Signal* **2011**, *4*, ra13.

(10) Zhang, Y.; Commisso, C. Macropinocytosis in Cancer: A Complex Signaling Network. *Trends Cancer* **2019**, *5*, 332−334.

(11) Patra, C. R.; Bhattacharya, R.; Wang, E.; Katarya, A.; Lau, J. S.; Dutta, S.; Muders, M.; Wang, S.; Buhrow, S. A.; Safgren, S. L.; et al. Targeted delivery of gemcitabine to pancreatic adenocarcinoma using cetuximab as a targeting agent. *Cancer Res.* **2008**, *68*, 1970−1978.

(12) Yan, Y.; Gause, K. T.; Kamphuis, M. M.; Ang, C. S.; O'Brien-Simpson, N. M.; Lenzo, J. C.; Reynolds, E. C.; Nice, E. C.; Caruso, F. Differential roles of the protein corona in the cellular uptake of nanoporous polymer particles by monocyte and macrophage cell lines. *ACS Nano* **2013**, *7*, 10960−10970.

(13) Giri, K.; Shameer, K.; Zimmermann, M. T.; Saha, S.; Chakraborty, P. K.; Sharma, A.; Arvizo, R. R.; Madden, B. J.; McCormick, D. J.; Kocher, J. P.; et al. Understanding protein-nanoparticle interaction: a new gateway to disease therapeutics. *Bioconjug Chem.* **2014**, *25*, 1078−1090.

(14) Arvizo, R. R.; Saha, S.; Wang, E.; Robertson, J. D.; Bhattacharya, R.; Mukherjee, P. Inhibition of tumor growth and metastasis by a self-therapeutic nanoparticle. *Proc. Natl. Acad. Sci. U. S. A.* **2013**, *110*, 6700−6705.

(15) Jain, R. K. Normalization of tumor vasculature: an emerging concept in antiangiogenic therapy. *Science* **2005**, *307*, 58−62.

(16) Saha, S.; Xiong, X.; Chakraborty, P. K.; Shameer, K.; Arvizo, R. R.; Kudgus, R. A.; Dwivedi, S. K.; Hossen, M. N.; Gillies, E. M.; Robertson, J. D.; et al. Gold Nanoparticle Reprograms Pancreatic Tumor Microenvironment and Inhibits Tumor Growth. *ACS Nano* **2016**, *10*, 10636−10651.

(17) Commisso, C.; Flinn, R. J.; Bar-Sagi, D. Determining the macropinocytic index of cells through a quantitative image-based assay. *Nat. Protoc* **2014**, *9*, 182−192.

(18) Means, N.; Elechalawar, C. K.; Chen, W. R.; Bhattacharya, R.; Mukherjee, P. Revealing macropinocytosis using nanoparticles. *Mol. Aspects Med.* **2022**, *83*, 100993.

(19) Xiong, X.; Rao, G.; Roy, R. V.; Zhang, Y.; Means, N.; Dey, A.; Tsaliki, M.; Saha, S.; Bhattacharyya, S.; Dhar Dwivedi, S. K.; et al. Ubiquitin-binding associated protein 2 regulates KRAS activation and macropinocytosis in pancreatic cancer. *Faseb j* **2020**, *34*, 12024−12039.

(20) Buscail, L.; Bournet, B.; Cordelier, P. Role of oncogenic KRAS in the diagnosis, prognosis and treatment of pancreatic cancer. *Nat. Rev. Gastroenterol Hepatol* **2020**, *17*, 153−168.

(21) Missero, C.; Pirro, M. T.; Di Lauro, R. Multiple ras downstream pathways mediate functional repression of the homeobox gene product TTF-1. *Mol. Cell. Biol.* **2000**, *20*, 2783−2793.
(22) Yuryev, A.; Wennogle, L. P. The RAF family: an expanding network of post-translational controls and protein-protein interactions. *Cell Res.* **1998**, *8*, 81−98.
(23) Hossen, M. N.; Wang, L.; Dwivedi, S. K. D.; Zhang, Y.; Rao, G.; Elechalwar, C. K.; Sheth, V.; Dey, A.; Asfa, S.; Gulla, S. K.; et al. Gold Nanoparticles Disrupt the IGFBP2/mTOR/PTEN Axis to Inhibit Ovarian Cancer Growth. *Adv. Sci. (Weinh)* **2022**, *9*, No. e2200491.
(24) Kudgus, R. A.; Walden, C. A.; McGovern, R. M.; Reid, J. M.; Robertson, J. D.; Mukherjee, P. Tuning pharmacokinetics and biodistribution of a targeted drug delivery system through incorporation of a passive targeting component. *Sci. Rep* **2014**, *4*, 5669.
(25) Hofmann, M. H.; Gerlach, D.; Misale, S.; Petronczki, M.; Kraut, N. Expanding the Reach of Precision Oncology by Drugging All KRAS Mutants. *Cancer Discov* **2022**, *12*, 924−937.
(26) Bannoura, S. F.; Uddin, M. H.; Nagasaka, M.; Fazili, F.; Al-Hallak, M. N.; Philip, P. A.; El-Rayes, B.; Azmi, A. S. Targeting KRAS in pancreatic cancer: new drugs on the horizon. *Cancer Metastasis Rev.* **2021**, *40*, 819−835.
(27) Schmick, M.; Vartak, N.; Papke, B.; Kovacevic, M.; Truxius, D. C.; Rossmannek, L.; Bastiaens, P. I. H. KRas localizes to the plasma membrane by spatial cycles of solubilization, trapping and vesicular transport. *Cell* **2014**, *157*, 459−471.
(28) Veithen, A.; Cupers, P.; Baudhuin, P.; Courtoy, P. J. v-Src induces constitutive macropinocytosis in rat fibroblasts. *J. Cell Sci.* **1996**, *109* (Pt 8), 2005−2012.
(29) Kimmelman, A. C. Metabolic Dependencies in RAS-Driven Cancers. *Clin. Cancer Res.* **2015**, *21*, 1828−1834.
(30) Zhang, Y.; Elechalawar, C. K.; Yang, W.; Frickenstein, A. N.; Asfa, S.; Fung, K.-M.; Murphy, B. N.; Dwivedi, S. K.; Rao, G.; Dey, A.; et al. Disabling partners in crime: Gold nanoparticles disrupt multicellular communications within the tumor microenvironment to inhibit ovarian tumor aggressiveness. *Mater. Today* **2022**, *56*, 79−95.
(31) Sauvage, F.; Fraire, J. C.; Remaut, K.; Sebag, J.; Peynshaert, K.; Harrington, M.; Van de Velde, F. J.; Xiong, R.; Tassignon, M. J.; Brans, T.; et al. Photoablation of Human Vitreous Opacities by Light-Induced Vapor Nanobubbles. *ACS Nano* **2019**, *13*, 8401−8416.
(32) Hou, K.; Zhao, J.; Wang, H.; Li, B.; Li, K.; Shi, X.; Wan, K.; Ai, J.; Lv, J.; Wang, D.; et al. Chiral gold nanoparticles enantioselectively rescue memory deficits in a mouse model of Alzheimer's disease. *Nat. Commun.* **2020**, *11*, 4790.
(33) Balfourier, A.; Kolosnjaj-Tabi, J.; Luciani, N.; Carn, F.; Gazeau, F. Gold-based therapy: From past to present. *Proc. Natl. Acad. Sci. U. S. A.* **2020**, *117*, 22639−22648.
(34) Seaberg, J.; Clegg, J. R.; Bhattacharya, R.; Mukherjee, P. Self-therapeutic nanomaterials: Applications in biology and medicine. *Mater. Today* **2023**, *62*, 190−224.
(35) Suk, J. S.; Xu, Q.; Kim, N.; Hanes, J.; Ensign, L. M. PEGylation as a strategy for improving nanoparticle-based drug and gene delivery. *Adv. Drug Deliv Rev.* **2016**, *99*, 28−51.
(36) Verhoef, J. J.; Anchordoquy, T. J. Questioning the Use of PEGylation for Drug Delivery. *Drug Deliv Transl Res.* **2013**, *3*, 499−503.
(37) Ivanov, M. R.; Bednar, H. R.; Haes, A. J. Investigations of the mechanism of gold nanoparticle stability and surface functionalization in capillary electrophoresis. *ACS Nano* **2009**, *3*, 386−394.
(38) Lu, A.; Tebar, F.; Alvarez-Moya, B.; Lopez-Alcala, C.; Calvo, M.; Enrich, C.; Agell, N.; Nakamura, T.; Matsuda, M.; Bachs, O. A clathrin-dependent pathway leads to KRas signaling on late endosomes en route to lysosomes. *J. Cell Biol.* **2009**, *184*, 863−879.
(39) Minoura, I.; Muto, E. Dielectric measurement of individual microtubules using the electroorientation method. *Biophys. J.* **2006**, *90*, 3739−3748.
(40) Elechalawar, C. K.; Hossen, M. N.; McNally, L.; Bhattacharya, R.; Mukherjee, P. Analysing the nanoparticle-protein corona for potential molecular target identification. *J. Controlled Release* **2020**, *322*, 122−136.
(41) Bhattacharyya, S.; Singh, R. D.; Pagano, R.; Robertson, J. D.; Bhattacharya, R.; Mukherjee, P. Switching the targeting pathways of a therapeutic antibody by nanodesign. *Angew. Chem., Int. Ed. Engl.* **2012**, *51*, 1563−1567.
(42) Arvizo, R. R.; Giri, K.; Moyano, D.; Miranda, O. R.; Madden, B.; McCormick, D. J.; Bhattacharya, R.; Rotello, V. M.; Kocher, J. P.; Mukherjee, P. Identifying new therapeutic targets via modulation of protein corona formation by engineered nanoparticles. *PLoS One* **2012**, *7*, No. e33650.

https://doi.org/10.1021/acsnano.3c00920
ACS Nano XXXX, XXX, XXX−XXX